Earthq Eng & Eng Vib (2008) 7:383-393 **DOI**: 10.1007/s11803-008-1010-9

Experimental verification of bridge seismic damage states quantified by calibrating analytical models with empirical field data

Swagata Banerjee† and Masanobu Shinozuka‡

Department of Civil and Environmental Engineering, University of California, Irvine, CA, USA

Abstract: Bridges are one of the most vulnerable components of a highway transportation network system subjected to earthquake ground motions. Prediction of resilience and sustainability of bridge performance in a probabilistic manner provides valuable information for pre-event system upgrading and post-event functional recovery of the network. The current study integrates bridge seismic damageability information obtained through empirical, analytical and experimental procedures and quantifies threshold limits of bridge damage states consistent with the physical damage description given in HAZUS. Experimental data from a large-scale shaking table test are utilized for this purpose. This experiment was conducted at the University of Nevada, Reno, where a research team from the University of California, Irvine, participated. Observed experimental damage data are processed to identify and quantify bridge damage states in terms of rotational ductility at bridge column ends. In parallel, a mechanistic model for fragility curves is developed in such a way that the model can be calibrated against empirical fragility curves that have been constructed from damage data obtained during the 1994 Northridge earthquake. This calibration quantifies threshold values of bridge damage states and makes the analytical study consistent with damage data observed in past earthquakes. The mechanistic model is transportable and applicable to most types and sizes of bridges. Finally, calibrated damage state definitions are compared with that obtained using experimental findings. Comparison shows excellent consistency among results from analytical, empirical and experimental observations.

Keywords: highway bridges; nonlinear time history analysis; fragility curves; threshold damage limits; mechanistic model; calibration

1 Introduction

Highway transportation networks consisting of various components such as bridges, roadways, tunnels and retaining walls, are spatially distributed over a wide geographical region. These systems are generally vulnerable to extreme natural hazards. For the seismic performance evaluation of such a distributed system, it is essential to have damageability information of all of its components, particularly bridges. With a proper knowledge of the degree of damage sustained by all constituent bridges, post-earthquake system degradation can be predicted satisfactorily and associated economic loss can be estimated. In this context, the most convenient way of expressing bridge seismic damageability is in a probabilistic manner that facilitates prediction of bridge failure probabilities in future earthquakes. Indeed, seismic fragility curves for various states of bridge damage are widely used in the framework of regional seismic risk evaluation of highway transportation systems.

Bridge fragility curves are usually developed using bridge damage data from various sources such as past earthquakes, analytical studies that numerically simulate bridge dynamic characteristics, and full-scale experimental studies. Detailed information about bridge physical damage observed during past earthquakes can be found in earthquake reconnaissance reports. These damage data can be categorized in various damage states such as "none," "minor," "moderate," "major" and "collapse" as defined in HAZUS (1999). Over the last decade, researchers have conducted studies to develop bridge fragility curves by statistically analysing empirical damage data (Shinozuka *et al*., 2000, 2003; Yamazaki *et al*., 2000; Tanaka *et al*., 2000; Basöz and Kiremidjian, 1998). In a very similar fashion, analytical fragility curves have also been developed utilizing damage data obtained through numerical simulation of bridge seismic response (Shinozuka *et al*., 2000, 2003, 2007; Nielson and DesRoches, 2007; Hwang *et al*., 2001; Basöz and Mander, 1999). However, in the later case, inconsistencies arise related to the definition and quantification of bridge damage states, since no standardized quantitative definition is available in accordance with the physical description of damage

Correspondence to: Swagata Banerjee, Department of Civil and Environmental Engineering, University of California, Irvine, E4130 Engineering Gateway, Irvine
Tel: (949) 824-9387; Fax: (949) 824-9389
E-mail: swagata@uci.edu
†Post-Doctoral Researcher; ‡Distinguished Professor and Chair

Supported by: Multidisciplinary Center for Earthquake Engineering Research, Contract No. R271883
Received October 30, 2008; **Accepted**: November 13, 2008

given in HAZUS (1999). Moreover, analytical fragility curves must be constructed in such a way that they can be used to numerically simulate the actual system degradation when an earthquake strikes a highway transportation network.

Hence, the quantification of bridge damage states is of primary importance, as this is one of the basic steps when analytically developing bridge fragility curves at different damage levels. Developed fragility curves will then be used in predicting the performance of highway bridges under future scenario earthquakes. The current study aims to quantify and verify bridge damage states by utilizing damage data obtained from all possible sources, e.g., empirical, experimental and analytical simulation. First, this study uses the damage data observed during a large-scale shaking table test conducted at the University of Nevada, Reno (Johnson *et al*., 2006) in which a research team from the University of California, Irvine, participated. The results of this experimental study (Johnson *et al*., 2006) included bridge response and the nature of its progressive failure under ground motions with various intensity levels. Damage data from this experiment is further analyzed here to obtain threshold limits (upper and lower bounds) of each damage state in terms of rotational ductility at column ends. In the second phase of this paper, bridge damage state definitions are quantified by performing mechanistic calibration of analytical bridge damage data with that observed during the 1994 Northridge earthquake. In this way, quantified damage states are consistent with the physical descriptions presented in HAZUS (1999). A comparison is performed in the third phase of this paper in which quantified damage states are verified with damage state definitions obtained from experimental observations.

2 Experimental study at the University of Nevada, Reno

A large-scale shaking table test of a 20.5 m long two-span reinforced concrete bridge model was conducted at the University of Nevada, Reno (Johnson *et al*., 2006). The total height of this specimen was 3.28 m from the bottom of the footing block to the top of the superstructure. Bridge spans, each 9.14 m long, were supported on three column bents with the tallest one at middle. Clear heights of these bents were 1.83 m, 2.44 m and 1.52 m. Each bent consisted of two columns of the same cross-sectional and material properties. The bridge deck was a solid slab post-tensioned in both the longitudinal and transverse directions of the bridge. Cast-in-place, drilled pile shafts were assumed for the foundations. Fig. 1 shows the bridge model. The axial force is estimated to be 209.2 kN in bent 1 and 3, and 182.2 kN in bent 2. More information about the bridge model can be found in Johnson *et al*. (2006). Damage data from this experiment is utilized in the current study to produce relevant results so that these can be compared with calibrated rotational ductility values obtained in succeeding sections.

2.1 Low and high amplitude tests

The bridge model was excited with both low and high amplitude earthquakes by placing it on three shaking tables. The ground motions used in this study were calculated from the motions recorded at the Century City Country Club during the 1994 Northridge earthquake. In this experiment, ground motions were only applied in the transverse direction of the bridge.

Before the high amplitude tests were undertaken, 11 tests were conducted in such a way that the longitudinal reinforcement in the columns did not yield. These tests are referred to as the low amplitude tests. Nine high amplitude tests were then performed (Tests 12 to 20) by gradually increasing the ground motion intensity. The main purpose of these high amplitude tests was to excite the model so that the columns failed in the transverse direction. To investigate the nature of progressive failure, the response of the bridge was recorded at each step, from yielding to buckling of the longitudinal reinforcement. In doing so, a ground motion with very low amplitude was applied during Test 12 and then scaled up gradually in consecutive tests. Table 1 lists target peak ground accelerations (PGAs) for the shaking tables during the high amplitude tests. The bridge was regarded to have failed during Test 19 when the columns

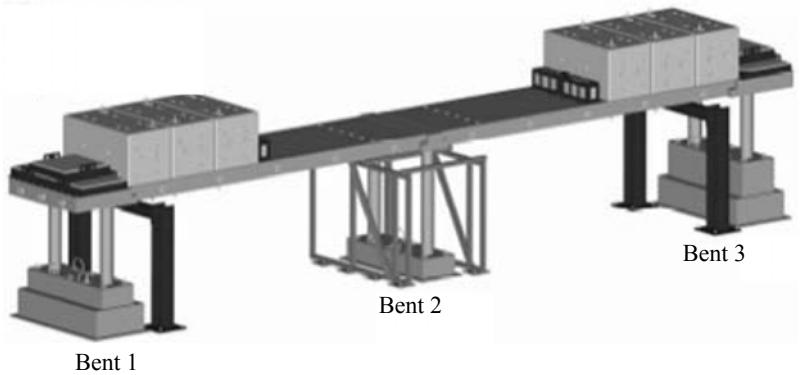

Fig. 1 Experimental model of a two-span reinforced concrete bridge (Johnson *et al*., 2006)

Table 1 Target PGAs in high amplitude tests

High amplitude tests	12	13	14	15	16	17	18	19	20
Target PGA for shaking tables (g)	0.075	0.15	0.25	0.50	0.75	1.00	1.33	1.66	1.00

of bent 3 failed in flexure, though no major damage was observed in other two bents. Upon completion of Test 20, two additional tests were performed with reduced amplitude to produce more damage in bents 1 and 2.

2.2 Bridge response and progressive damage in columns

Prior to testing, the model was instrumented with displacement transducers, accelerometers and strain gauges in order to record its response. Johnson *et al*. (2006) documents this response in terms of displacement and acceleration of superstructure, curvature at column ends, and strain in the column reinforcement.

Recorded response during the high amplitude tests indicates a pattern of progressive failure for the bridge. Damage is mainly observed at both ends of bridge columns. During Tests 12 and 13, no damage was observed in any of the columns. Gradually, hairline cracks started to form in the cover concrete during Test 14, though no significant damage was noticed at that time. During Tests 15 and 16, cover concrete in columns started to spall and this became significant during Test 17. During Test 19, both columns of bent 3 failed in flexure due to the buckling of the longitudinal reinforcing steel. At this stage, plastic hinges had formed at both ends (top and bottom) of the columns in bent 3, and spiral reinforcement had fractured at some locations. Readers are referred to Johnson *et al*. (2006) for a detailed description of this progressive failure and the observed damage in the columns.

3 Identification of damage states from experimental results

The current study utilizes rotational ductility at column ends as the parameter to characterize the bridge damage states. Threshold damage limits representing the upper and lower bounds are estimated for minor, moderate and major damage levels. Such bounds are evaluated in this paper by utilizing observed damage data from the above-mentioned experiment. For this purpose, bridge damage states are introduced as no such definition is used in Johnson *et al*. (2006) for the experimental damage data. Experimental damage data are then categorized into these newly incorporated damage states as detailed in subsequent sections of this paper.

3.1 Bridge damage states

According to the nature and severity of the damage observed in the columns during the high amplitude tests, this damage is categorized into four damage levels, namely no damage, minor damage, moderate damage and major damage. Table 2 lists these states and corresponding damage descriptions as given in HAZUS (1999). Following this, engineering judgment is applied to develop guidelines by means of which observed experimental data from Johnson *et al*. (2006) are actually categorized into different damage states.

At the beginning of the high amplitude tests (during Tests 12 to 14), no damage was observed in the columns. Therefore, observed curvatures at column ends during these initial tests represent the state of no damage. In a similar fashion, recorded curvatures at bridge column ends are categorized in minor, moderate and major damage states. Table 3 lists curvatures at column ends observed during the high amplitude tests and the corresponding damage levels in the bridge.

3.2 Moment-rotation analysis

From the experimental results (Johnson *et al*., 2006), seismic response may be determined in terms of

Table 2 Bridge damage as observed from the experiment

Damage states	Descriptions of damage given in HAZUS (1999)	Descriptions of damage observed in the experiment (Johnson *et al*., 2006)
None	No damage	No damage in columns
Minor	Minor cracking and spalling to abutments, hinges, columns or minor cracking to the deck	Extent of spalling of concrete cover ≤ 80 mm
Moderate	Any column experiencing moderate cracking and spalling (column structurally still sound), any connection having cracked shear keys or bent bolts, or moderate settlement of the approach	Extent of spalling of concrete cover > 80 mm and exposure of column reinforcement
Major	Any column degrading without collapse (column structurally unsafe), any connection losing some bearing support, or major settlement of the approach	Buckling of reinforcing bar(s); formation of plastic hinge(s)

Table 3 Recorded curvatures at column ends (Johnson *et al*., 2006) and corresponding damage levels

East column in bents			West column in bents		
Location	Test #	Curvature (rad/mm)	Location	Test #	Curvature (rad/mm)
		No damage			
Bent 1, Top	12	1.1×10^{-5}	Bent 1, Top	12	1.3×10^{-5}
	14	4.4×10^{-5}		14	4.5×10^{-5}
Bottom	12	1.3×10^{-5}	Bottom	12	1.4×10^{-5}
	15	1.0×10^{-4}		15	1.2×10^{-4}
Bent 2, Top	12	5.4×10^{-6}	Bent 2, Top	12	6.0×10^{-6}
	15	4.2×10^{-5}		15	4.8×10^{-5}
Bottom	12	8.8×10^{-6}	Bottom	12	7.4×10^{-6}
	15	5.2×10^{-5}		16	1.3×10^{-4}
Bent 3, Top	12	9.8×10^{-6}	Bent 3, Top	12	9.0×10^{-6}
	14	3.9×10^{-5}		15	7.3×10^{-5}
Bottom	12	1.0×10^{-5}	Bottom	12	1.1×10^{-5}
	14	4.0×10^{-5}		14	4.0×10^{-5}
		Minor damage			
Bent 1, Top	16	1.8×10^{-4}	Bent 1, Top	16	2.0×10^{-4}
	17	1.4×10^{-4}		18	2.3×10^{-4}
Bottom	16	2.2×10^{-4}	Bottom	16	2.1×10^{-4}
	17	1.7×10^{-4}		17	1.5×10^{-4}
Bent 2, Top	18	2.0×10^{-4}	Bent 2, Top	19	2.4×10^{-4}
Bottom	18	1.7×10^{-4}	Bottom	18	1.9×10^{-4}
Bent 3, Top	15	1.3×10^{-4}	Bent 3, Top	16	1.5×10^{-4}
	16	1.9×10^{-4}			
Bottom	15	1.4×10^{-4}	Bottom	16	2.0×10^{-4}
	16	2.0×10^{-4}		15	1.5×10^{-4}
		Moderate damage			
Bent 1, Top	19	2.7×10^{-4}	Bent 1, Top	19	2.9×10^{-4}
	21	2.4×10^{-4}			
Bottom	19	3.2×10^{-4}	Bottom	19	3.0×10^{-4}
	21	2.4×10^{-4}			
Bent 2, Top	22	2.8×10^{-4}	Bent 2, Top	22	3.0×10^{-4}
Bottom	22	2.5×10^{-4}	Bottom	22	3.2×10^{-4}
Bent 3, Top	18	3.4×10^{-4}	Bent 3, Top	18	2.6×10^{-4}
Bottom	18	3.7×10^{-4}	Bottom	18	3.2×10^{-4}
		Major damage			
Bent 3, Top	19	5.3×10^{-4}	Bent 3 Top	19	4.6×10^{-4}
	21	3.9×10^{-4}		20	3.8×10^{-4}
Bottom	19	5.0×10^{-4}	Bottom	20	4.6×10^{-4}
	21	4.0×10^{-4}			

rotation, displacement, and acceleration. However, for the purpose of comparison, it is necessary to evaluate rotational ductility from these observed curvatures at bridge column ends. This can be done once the yield and ultimate curvatures of bridge columns are known. The moment-curvature relationship of bridge columns presented in Johnson *et al*. (2006) provides conservative estimate in comparison to the experimental observations. For example, the ultimate curvature obtained from the moment-curvature relationship given in this report (Page

70, Paragraph 3 of Johnson *et al*., 2006) is 0.00028 rad/mm, while a maximum curvature of 0.00037 rad/mm is observed in columns of bent 3 during Test 18. Again, in Test 19 when these columns are sustaining major damage in the sense that they buckled in flexure, the observed curvature is nearly twice the ultimate curvature obtained from the moment-curvature analysis by Johnson *et al*. (2006). Therefore, these moment-curvature relationships cannot be used for computing the yield and ultimate curvatures of the columns.

For this reason, the present study develops the moment-rotation relationships for these columns by utilizing the program given by Kushiyama (2002), which follows the theoretical formulation presented in Priestley *et al*. (1996). To run this program, input data such as effective column height, column diameter, concrete cover, number and diameter of longitudinal reinforcing bars, and diameter and spacing of spiral reinforcement are obtained from the column reinforcement plan (Fig. 2-4, Page 223 of Johnson *et al*., 2006). Table 4 lists all of these required input parameters for the current moment-rotation analysis. Figures 2 and 3 show the moment-rotation relationships of individual columns in three bents. These curves give better results for the ultimate rotations than Johnson *et al.* (2006), and are comparable with the ultimate rotations observed in the experiment during Test 19.

3.3 Rotational ductility of bridge columns at various damage states

According to the experimental set-up, rotations at bridge column ends are calculated by multiplying recorded curvature (Table 3) with gauge length (127 mm). This gauge length is the interval between curvature rod and fixity (Johnson *et al*., 2006). Rotational ductility is estimated by dividing rotations at bridge column ends with yield rotations obtainable from moment-rotation relation of column bents (Figs. 2 and 3). Table 5 presents rotations at column ends and corresponding rotational ductility values. In this table, values in bold and italic letters represent maximum or minimum rotational ductility obtained at different bridge damage states.

The rotational ductility values from Table 5 are plotted in Fig. 4 for four damage levels. In this figure, damage state index 0, 1, 2 and 3, respectively, represent no, minor, moderate and major damage states. Threshold damage limits are estimated by averaging minimum and maximum rotational ductilities observed in two successive damage levels. For example, minimum rotational ductility observed in minor damage is 3.27 while the maximum rotational ductility observed in no damage is 3.01. Therefore, lower bound of rotational ductility for the state of minor damage is computed as 3.14. Similar values for the thresholds of moderate

Table 4 Input parameters for moment-curvature analysis of columns

Effective height of members	Diameter of bridge columns	Axial force by dead load	
H_{bent1} amd H_{bent3} = 2.58 m, H_{bent2} = 3.19 m	0.3048 m	209.2 kN (bent 1 and 3), 182.2 kN (bent 2)	
Compressive strength of unconfined concrete	Yield stress of longitudinal reinforcement	Yield stress of hoop reinforcement	Concrete cover to confine longitudinal reinforcement
34.42 MPa	457.85 MPa	461.30 MPa	19 mm
Number of longitudinal bars	Diameter of longitudinal bars	Diameter of hoops	Spacing of hoops
16	9.525 mm (#3)	4.88 mm (W2.9)	31.75 mm

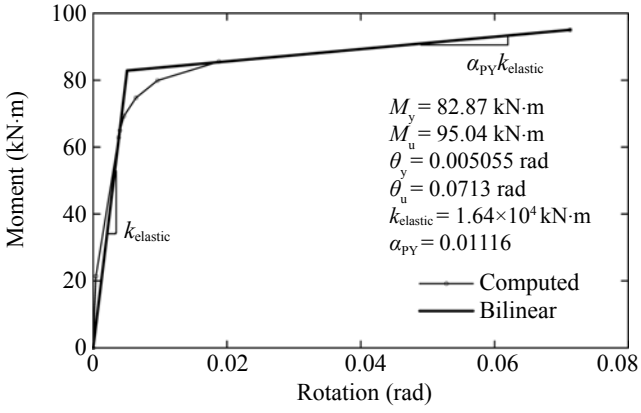

Fig. 2 Moment-rotation relationship of each column in Bent 1 and Bent 3

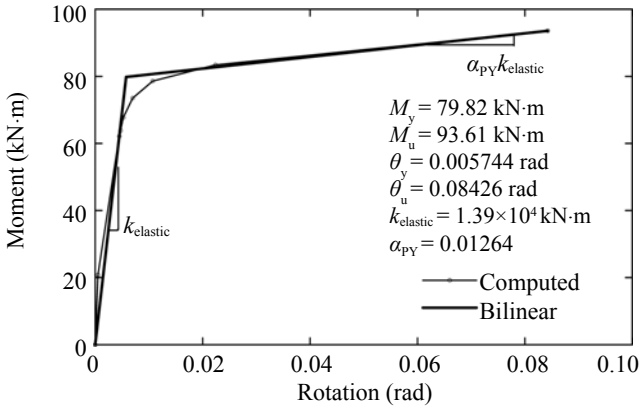

Fig. 3 Moment-rotation relationship of each column in Bent 2

Table 5 Rotational ductility of bridge columns at different damage levels

East column in bent				West column in bent			
Location	Curvature (rad / mm)	Rotation (rad)	Rot. ductility	Location	Curvature (rad / mm)	Rotation (rad)	Rot. ductility
No damage							
Bent 1	1.1×10^{-5}	0.0014	0.28	Bent 1	1.3×10^{-5}	0.0017	0.33
	4.4×10^{-5}	0.0056	1.11		4.5×10^{-5}	0.0057	1.13
	1.3×10^{-5}	0.0017	0.33		1.4×10^{-5}	0.0018	0.35
	1.0×10^{-4}	0.0127	2.51		1.2×10^{-4}	0.0152	***3.01***
Bent 2	5.4×10^{-6}	0.0007	***0.12***	Bent 2	6.0×10^{-6}	0.0008	0.13
	4.2×10^{-5}	0.0053	0.93		4.8×10^{-5}	0.0061	1.06
	8.8×10^{-6}	0.0011	0.19		7.4×10^{-6}	0.0009	0.16
	5.2×10^{-5}	0.0066	1.15		1.3×10^{-4}	0.0165	2.87
Bent 3	9.8×10^{-6}	0.0012	0.25	Bent 3	9.0×10^{-6}	0.0011	0.23
	3.9×10^{-5}	0.0050	0.98		7.3×10^{-5}	0.0093	1.83
	1.0×10^{-5}	0.0013	0.25		1.1×10^{-5}	0.0014	0.28
	4.0×10^{-5}	0.0051	1.00		4.0×10^{-5}	0.0051	1.00
Minor damage							
Bent 1	1.8×10^{-4}	0.0229	4.52	Bent 1	2.0×10^{-4}	0.0254	5.02
	1.4×10^{-4}	0.0178	3.52		2.3×10^{-4}	0.0292	***5.78***
	2.2×10^{-4}	0.0279	5.53		2.1×10^{-4}	0.0267	5.28
	1.7×10^{-4}	0.0216	4.27		1.5×10^{-4}	0.0191	3.77
Bent 2	2.0×10^{-4}	0.0254	4.42	Bent 2	2.4×10^{-4}	0.0305	5.31
	1.7×10^{-4}	0.0216	3.76		1.9×10^{-4}	0.0241	4.20
Bent 3	1.3×10^{-4}	0.0165	***3.27***	Bent 3	1.5×10^{-4}	0.0191	3.77
	1.9×10^{-4}	0.0241	4.77		2.0×10^{-4}	0.0254	5.02
	1.4×10^{-4}	0.0178	3.52		1.5×10^{-4}	0.0191	3.77
	2.0×10^{-4}	0.0254	5.02				
Moderate damage							
Bent 1	2.7×10^{-4}	0.0343	6.78	Bent 1			
	2.4×10^{-4}	0.0305	6.03		2.9×10^{-4}	0.0368	7.29
	3.2×10^{-4}	0.0406	8.04		3.0×10^{-4}	0.0381	7.54
	2.4×10^{-4}	0.0305	***6.03***				
Bent 2	2.8×10^{-4}	0.0356	6.19	Bent 2	3.0×10^{-4}	0.0381	6.63
	2.5×10^{-4}	0.0318	5.53		3.2×10^{-4}	0.0406	7.08
Bent 3	3.4×10^{-4}	0.0432	8.54	Bent 3	2.6×10^{-4}	0.0330	6.53
	3.7×10^{-4}	0.0470	***9.30***		3.2×10^{-4}	0.0406	8.04
Major Damage							
Bent 3	5.3×10^{-4}	0.0673	***13.32***	Bent 3	4.6×10^{-4}	0.0584	11.56
	3.9×10^{-4}	0.0495	9.80		3.8×10^{-4}	0.0483	***9.55***
	5.0×10^{-4}	0.0635	12.56		4.6×10^{-4}	0.0584	11.56
	4.0×10^{-4}	0.0508	10.05				

and major damage are estimated as 5.90 and 9.42, respectively. It should be noted here that these values of threshold limits are obtained considering all columns in the same statistical population.

4 Mechanistic quantification of bridge seismic damage states

As mentioned before, bridge damage data from past earthquakes is a valuable set of information. This empirical data is used in this study to calibrate analytical fragility curves such that analysis becomes consistent with global statistics of bridge damage. For this purpose, a mechanistic model is developed as described below. Readers are referred to Banerjee and Shinozuka (2008) for a detailed discussion.

4.1 Empirical fragility curves of Caltrans (California Department of Transportation) bridges

Damage reports of the 1994 Northridge Earthquake (Caltrans, 1994a, b) documented physical damage suffered by highway bridges in southern California and their corresponding damage states as minor, moderate, extensive (no collapse) and collapse as per the definition given in HAZUS (1999). Damage data from these reports is analyzed statistically to develop empirical fragility curves in four different subset levels, Level 1 to Level 4 (Shinozuka *et al*., 2000, 2003). These subset levels are formed by combining bridges with different attributes and configurations, such as span number, soil type and skew angle. A two-parameter lognormal distribution function is used to express the bridge fragility curve in which seismic intensity is characterized by peak ground acceleration (PGA). The maximum likelihood method is performed to estimate bridge fragility parameters (median, *c,* and log-standard deviation, ζ) at each state of bridge damage. Fragility curves are developed for 18 different bridge combinations in Level 4 subset. Among these, one set combining 720 bridges with 'multiple span,' skew angle '0° – 20°' and soil type 'C' are utilized in the current study for calibration purposes. This bridge combination is chosen because of its strong resemblance to the bridges used for the analytical studies (Bridges 1, 2 and 3) discussed later in this paper.

Selected bridge fragility curves, however, may have some uncertainty. This uncertainty comes from the fact that the empirical bridge damage data is based on the subjective judgment of the inspectors during post-earthquake reconnaissance. Therefore, statistical variations of these empirical fragility curves need to be examined prior to make any comparison. This is done by estimating 90% confidence intervals of empirical fragility parameters that correspond to their 5% and 95% exceedance probabilities. For this purpose, Monte Carlo simulation is performed to generate 512 realizations of median values at minor, moderate and major damage states (c_{1emp}, c_{2emp}, and c_{3emp}) and log-standard deviation (ζ_{emp}). Figure 5 shows these empirical curves at the three damage levels, where the curves towards the right side of the figure are for the higher damage levels. It should be noted that the log-standard deviation (ζ) is kept unaltered in all damage states so that any two fragility curves do not intersect with each other.

4.2 Development of analytical fragility curves

In order to develop analytical fragility curves, three bridges are analyzed subject to 60 ground motion time histories. These ground motions represent the wide range of seismic hazard in the Los Angeles region. Figure 6 shows these bridge models. The finite element computer code SAP2000 Nonlinear (Computers and Structures, Inc., 2002) is used to analyse these bridges in the time domain and their response is measured in

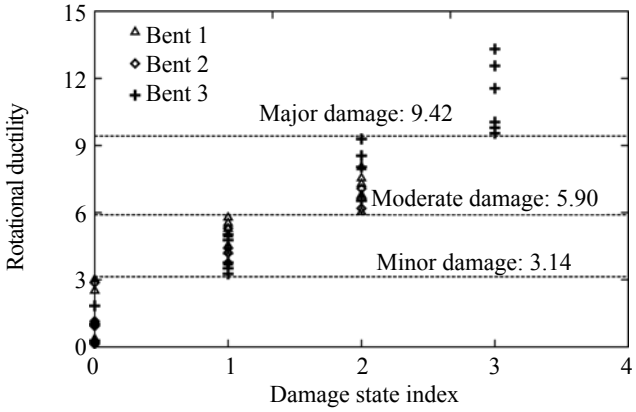

Fig. 4 Estimated rotational ductility values from experimental data

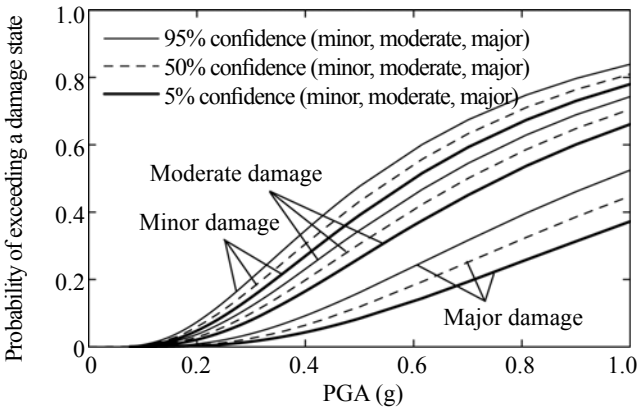

Fig. 5 Empirical fragility curves of bridges with 'multiple span,' skew angle '0° – 20°' and soil type 'C' at minor, moderate and major damage states with 95%, 50% and 5% statistical confidence (Banerjee and Shinozuka, 2008)

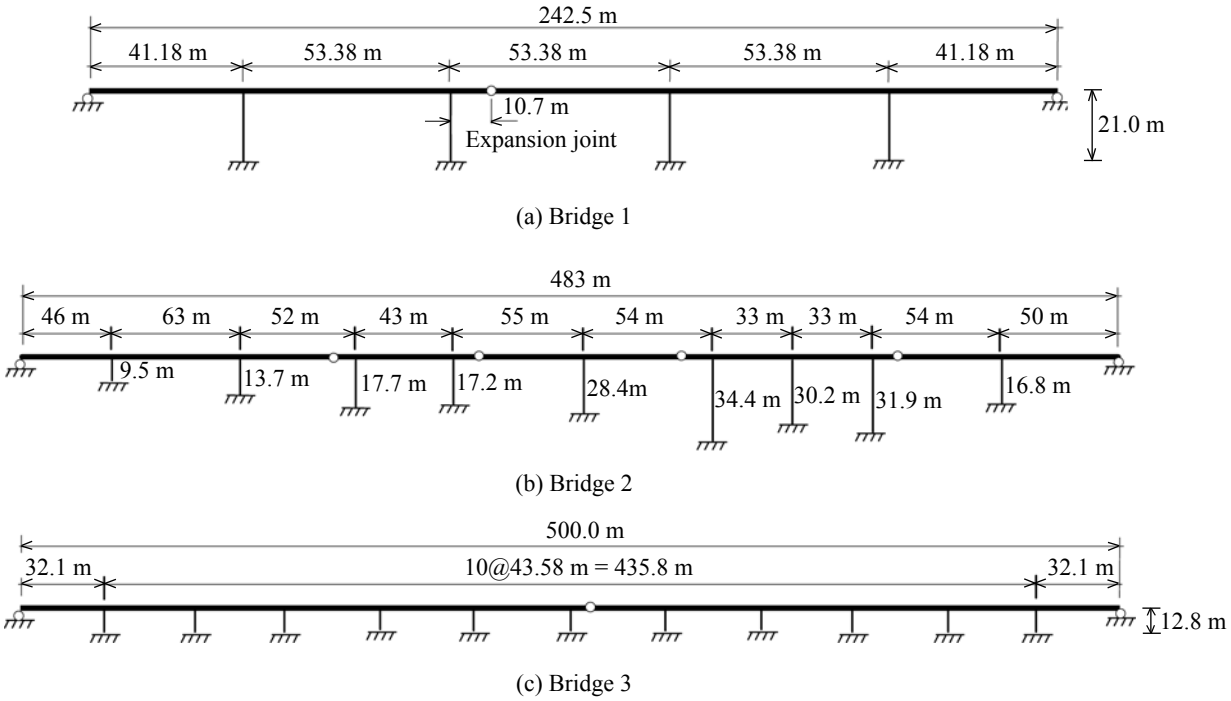

(a) Bridge 1

(b) Bridge 2

(c) Bridge 3

Fig. 6 Bridges used in derivation of analytical fragility curves

terms of rotation at column ends, pounding force at expansion joints, axial force in restrainers, and shear force at column ends. Readers are referred to Banerjee and Shinozuka (2008) for detailed information about the finite element modelling of these bridges and their seismic response obtained from nonlinear time history analysis.

A previous study on the progressive failure analysis of Bridge 1 in the time domain showed that failure at expansion joint is preceded by the formation of plastic hinges at column ends (Banerjee and Shinozuka, 2004). Therefore, rotational ductility at the column ends is taken as the governing parameter to characterize the bridge damage states, and eventually be used for fragility analysis. After generating bridge response, analytical fragility curves are developed by following the same procedure as used for empirical fragility curve development (Shinozuka *et al*., 2000 and 2003). Fig. 7 shows the analytical fragility curves derived for these bridges.

4.3 Comparison of fragility curves with empirical data

Empirical fragility curves for 90% confidence intervals (Fig. 5) may be used to evaluate the analytically developed fragility curves for the three sample bridges (Fig. 7). A comparison indicates that the analytical curves tend to provide a substantially more conservative result, in the sense that bridges are more likely to sustain a damage state than the empirical fragility curves suggest. As shown in Fig. 8, the probability that Bridge 1 will reach the state of minor damage at a PGA of 0.4g is 54% from the analytical curves, whereas this probability varies from 27% to 34.5% in the empirical curves with 90% confidence interval. Similar discrepancies are observed for all bridges and states of damage. However, these discrepancies can be minimized for each pair of empirical and analytical fragility curves associated with the same state of damage by mechanistically adjusting the minimum rotational ductility value and by utilizing the least square optimization procedure as mentioned in the following section. More detailed discussion about this calibration can be found in Banerjee and Shinozuka (2008).

4.4 Calibration of analytical fragility curves

To quantify bridge damage states in terms of rotational ductility at column ends, response from SAP2000 is used as input. For each damage state, a threshold ductility value is estimated that indicates the lower bound of that damage state. For this purpose, a MATLAB (MATLAB, 2004) computer code is developed in which two optimization procedures are performed simultaneously. In the first optimization, analytical fragility parameters are estimated by making an initial guess of the damage states in terms of rotational ductility. In the second optimization, the difference between the analytical and empirical fragility parameters is minimized and threshold ductility values are obtained.

The above procedure is performed independently for Bridges 1, 2 and 3. It calibrates the analytical fragility curves so that these curves become consistent with the

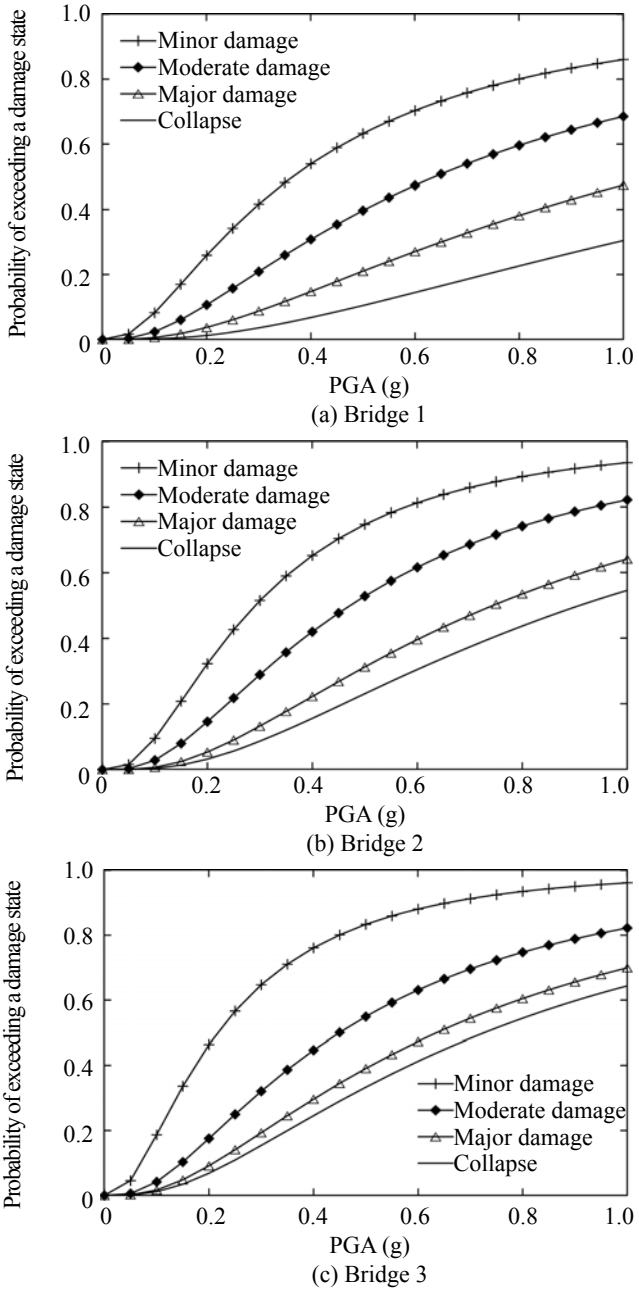

Fig. 7 Analytical fragility curves

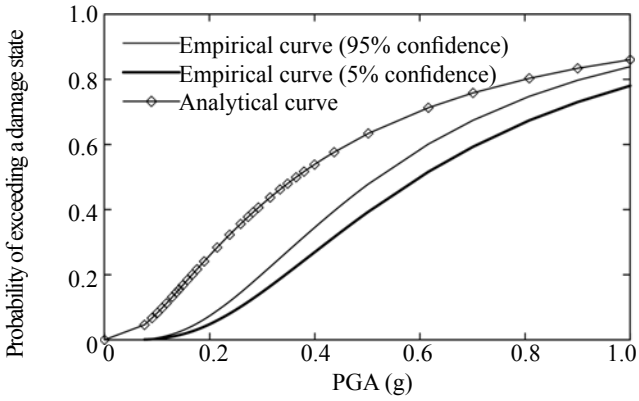

Fig. 8 Comparison of empirical and analytical fragility curves of bridge 1 for the state of minor damage

empirical results. Table 6 presents median values (*c*) for empirical fragility curves and calibrated analytical fragility curves. Results indicate that at minor and moderate damage states, calibrated median values fall into the 90% confidence bands of the corresponding empirical fragility curves, although differences are observed in the major damage states for Bridges 2 and 3. This is due, in part, to the fact that only a limited number of failure cases were obtained in the major damage state when analyzing these bridges. It is also due to the fact that only a few bridges suffered major damage or collapsed in the Northridge earthquake and the population of these bridges in the empirical database is small. Analysis with many severe ground motions, which may cause major damage to Bridges 2 and 3 may produce better correspondence with empirical data. In fact, the process of calibration discussed here represents a methodology. As knowledge about structural damage advances, more precise estimation of damage limits can be expected.

Estimated lower bounds of the calibrated rotational ductility capacities at all three damage states are presented in Table 7. Figure 9 shows these capacities for different damage states in which indices 1, 2, and

Table 6 Fragility parameters for empirical and calibrated analytical fragility curves

Damage states	Median values (g)				
	Empirical fragility curves		Calibrated analytical fragility curves		
	95% confidence	5% confidence	Bridge 1	Bridge 2	Bridge 3
Minor	0.52	0.60	0.56	0.54	0.53
Moderate	0.65	0.76	0.70	0.67	0.67
Major	0.96	1.24	1.06	0.83	0.73

Table 7 Lower bound of calibrated rotational ductility of bridges

Bridge No	Threshold rotational ductility at different damage states		
	Minor	Moderate	Major
1	3.39	4.75	8.43
2	6.43	9.02	12.35
3	5.93	9.06	12.18

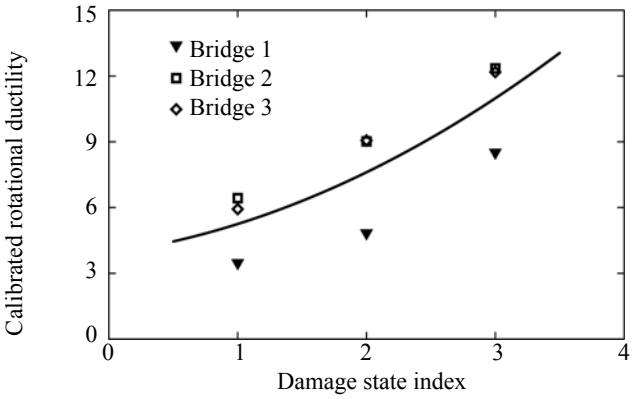

Fig. 9 Rotational ductility capacities at various damage states

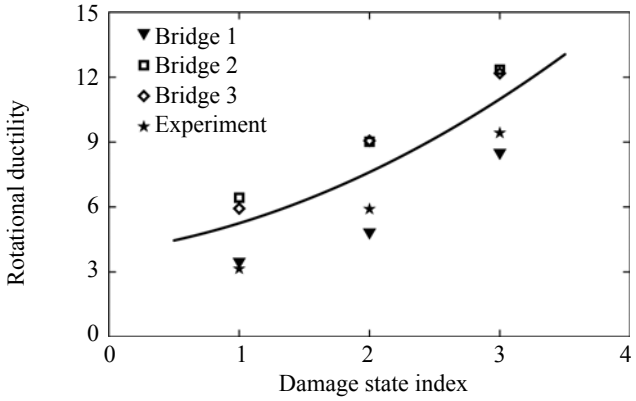

Fig. 10 Rotational ductilities representing threshold limits of bridge damage

3 stand for 'Minor Damage,' 'Moderate Damage' and 'Major Damage,' respectively. This figure shows that in all damage states, rotational ductility capacities for Bridges 2 and 3 almost overlap with each other while those for Bridge 1 lay far apart. This may be due to the fact that Bridges 2 and 3 are very similar in terms of their span number and overall length, whereas Bridge 1 is much smaller. For the purpose of calibration, these three analytical bridges are considered in the same bridge class, which is equivalent to one of the 18 empirical bridge classes in the Level 4 subset (Shinozuka *et al*., 2000 and 2003). Hence, it can be stated from this observation that a more detailed bridge classification is needed to categorize the empirical bridge damage data for it to be used to calibrate analytical fragility curves. For example, if empirical bridge damage data are classified according to bridge length, span numbers, type and height of columns, and foundation type, in addition to the existing categorization, mechanistic calibration may produce better agreement.

5 Comparison of threshold damage limits

The experimental model (Fig. 1) is a two-span bridge with zero skew and is comparable to those used for the analytical studies (Fig. 6). For the purpose of comparison, threshold damage limits derived from the experimental observations (Fig. 4) are plotted in Fig. 10 together with those obtained from the mechanistic calibration of the analytical damage models (Fig. 9). This comparison shows that the damage state limits obtained from the experimental results correspond satisfactorily with those obtained from mechanistic calibration. Thus, by integrating probabilistic, statistical and mechanistic aspects of bridge damageability, analytical damage states are calculated which are consistent with actual damage observed both in a natural event and a laboratory experiment.

6 Conclusions

This paper uses empirical, analytical and experimental seismic damage data of bridges to quantify and verify threshold damage limits in terms of rotational ductility in bridge columns. To perform this study, bridge damage data from a large-scale shaking table test is used. This damage data included bridge response (i.e., displacements and rotations) and observed physical damage at different locations. Recorded response quantities are further analyzed in this study to categorize them under different damage levels consistent with the HAZUS physical damage descriptions. This categorization produced threshold damage limits, by means of which, different bridge damage states are defined and quantified.

In a parallel process, an analytical study is performed in which three bridges are analyzed under 60 earthquake ground motions, and analytical fragility curves are generated. A mechanistic model is developed through which analytical fragility curves are calibrated with empirical bridge damage data from the 1994 Northridge earthquake. This calibration produced threshold values of rotational ductility that quantify bridge damage states in agreement with physical damage observed in past earthquake.

Obtained damage state definitions from the mechanistic model and experimental observation are compared to verify the analytical procedure. This comparison shows good correspondence between the threshold damage limits from the above two sources, which confirms the consistency of calibrated bridge damage states. Obviously, more precise measurement of these damage state definitions can be made using bridge damage data from other past earthquakes and/or from additional experimental studies with pertinent bridges.

Acknowledgements

This study was supported by Multidisciplinary Center for Earthquake Engineering Research (MCEER: Contract No. R271883). The authors are thankful to Professor M. Saiidi and Professor D.H. Sanders, University of Nevada, Reno (UNR) for sharing the results of the large-scale shake table experiment performed at UNR, in which a research team advised by Professor M. Feng, University of California, Irvine, also participated.

References

Banerjee S and Shinozuka M (2004), "Dynamic Progressive Failure of Bridges," *CD-Rom Proceeding of ASCE Joint Specialty Conference on Probabilistic Mechanics and Structural Reliability*, Albuquerque, New Mexico, USA.

Banerjee S and Shinozuka M (2008), "Mechanistic Quantification of RC Bridge Damage States Under Earthquake Through Fragility Analysis," *Probabilistic Engineering Mechanics*, **23**(1): 12–22.

Basöz N and Kiremidjian AS (1998), "Evaluation of Bridge Damage Data from the Loma Prieta and Northridge, California Earthquakes," *Technical Report MCEER-98-0004*, Multidisciplinary Center for Earthquake Engineering Research, State University of New York at Buffalo, USA.

Basöz N and Mander JB (1999), "Enhancement of the Highway Transportation Lifeline Module in HAZUS," *Final Pre-Publication Draft (#7)*, National Institute of Building Sciences.

Caltrans (1994a), "The Northridge Earthquake," *Caltrans Post Earthquake Investigation Report*, California Department of Transportation, Division of Structures, Sacramento, CA, USA.

Caltrans (1994b), "Supplementary Bridge Damage Reports," *Caltrans Report*, California Department of Transportation, Division of Structures, Sacramento, CA, USA.

Computers and Structures, Inc. (2002), *SAP2000 Nonlinear Users Manual*, V. 8, Berkeley, CA, USA.

HAZUS (1999), "Earthquake Loss Estimation Methodology," *Technical Manual SR2*, Federal Emergency Management Agency through agreements with National Institute of Building Science, Washington, D.C., USA.

Hwang H, Liu JB and Chiu YH (2001), "Seismic Fragility Analysis of Highway Bridges," *Technical Report*, Center for Earthquake Research and Information, University of Memphis, Tennessee, USA.

Johnson NS, Saiidi M and Sanders DH (2006), "Large-scale Experimental and Analytical Seismic Studies of a Two-Span Reinforced Concrete Bridge System," *Report No. CCEER-06-02*, Center for Earthquake Engineering Research, University of Nevada, Reno, NV, USA.

Kushiyama S (2002), "Calculation Moment-rotation Relationship of Reinforced Concrete Member with/ without Steel Jacket," *Internal Report at University of Southern California*, CA, USA.

MATLAB: Computing Environment for Technical Education (2004), The MathWorks, Inc., Prentice-hall, Englewood Cliffs, NJ, USA.

Neilson BG and DesRoches R (2007), "Seismic Fragility Methodology for Highway Bridges Using a Component Level Approach," *Earthquake Engineering and Structural Dynamics*, **36**(6): 823–839.

Priestley MJN, Seible F and Calvi GM (1996), *Seismic Design and Retrofit of Bridges*, NY: John Wiley and Sons.

Shinozuka M, Banerjee S and Kim SH (2007), "Statistical and Mechanistic Fragility Analysis of Reinforced Concrete Bridges," *Technical Report MCEER-07-0015*, Multidisciplinary Center for Earthquake Engineering Research, State University of New York at Buffalo.

Shinozuka M, Feng MQ, Kim H, Uzawa T and Ueda T (2003), "Statistical Analysis of Fragility Curves," *Technical Report MCEER-03-0002*, Multidisciplinary Center for Earthquake Engineering Research, State University of New York, Buffalo, USA.

Shinozuka M, Feng MQ, Lee J and Naganuma T (2000), "Statistical Analysis of Fragility Curves," *Journal of Engineering Mechanics*, ASCE, **126**(12): 1224–1231.

Tanaka S, Kameda H, Nojima N and Ohnishi S (2000), "Evaluation of Seismic Fragility for Highway Transportation Systems," *Proceedings of the 12th World Conference on Earthquake Engineering*, Upper Hutt, New Zealand, Paper No. 0546.

Yamazaki F, Motomura H and Hamada T (2000), "Damage Assessment of Expressway Networks in Japan Based on Seismic Monitoring," *Proceeding of the 12th World conference on Earthquake Engineering*, Upper Hutt, New Zealand, Paper No. 0551.